Effects of Temperature, Aerodynamic Straining and Suppressant Concentration on Catalytic Inhibition by CF_3Br in Methane-Air Counterflow Diffusion Flames

Yuko SASO and Naoshi SAITO

National Research Institute of Fire and Disaster
14-1 Nakahara 3-chome, Mitaka, Tokyo 181-8633, Japan

ABSTRACT

Effect of flame temperature on the efficiency of catalytic inhibition cycles by CF_3Br in methane-air counterflow diffusion flames are numerically investigated with detailed chemistry and transport. Computational results are compared with the previous finding of one-dimensional freely propagating flames, in which the efficiency of catalytic inhibition cycles with Br species is markedly enhanced at lower flame temperatures because of longer residence time in the reaction zone. The present results at constant strain rates demonstrate that the efficiency of inhibition cycles in the counterflow flame is enhanced at lower flame temperatures, while the residence time remains unchanged with the flame temperature variation. The enhanced efficiency in the counterflow flame is attributed to the slower oxidation, which results in higher concentrations of fuel-originated intermediates in the reaction zone, that are important for regeneration of HBr from Br. The effects of strain rate and CF_3Br concentration in the oxidizer are also examined. At a constant flame temperature, the efficiency of inhibition cycles is found to be greater at smaller strain rates and suppressant doping.

KEYWORDS: CF_3Br, halon 1301, halogenated suppressant, inhibition, inhibitor, temperature effect, strained flame, combustion modeling, fire suppression, extinction.

INTRODUCTION

Following the ban of halon production to protect the stratospheric ozone layer, effort has been made to search highly effective, new chemical suppressants. At the same time, the flame inhibition mechanisms of Halon 1301 (CF_3Br) have been investigated extensively to guide the search for replacement chemicals [1-5]. One of the most significant issues on CF_3Br is the role of catalytic cycles by which H atoms are considered to be recombined efficiently. Westbrook [1] demonstrated the H atom recombination catalyzed by the Br atom through numerical simulation. Noto et al. [2] introduced a regeneration coefficient, which quantifies the effective number of catalytic cycles per suppressant added to a flame, and determined it to be approximately 7 for atmospheric stoichiometric methane-air flame with 1% CF_3Br. On the other hand, Casias and McKinnon [5] showed that less than a single cycle is carried out in the time scale available in an ethylene-air flame, and concluded that catalytic cycles are not the predominant cause of inhibition by CF_3Br.

In addition to the above concern, several recent studies [6-9] demonstrated that the binary

mixtures of CF_3Br and inert gases (e.g., N_2, CO_2) show synergistic interactions on flame inhibition effectiveness. Because flame inhibition by inert gases is achieved mainly through flame temperature reduction, it was suggested [6-8] that the observed synergism of CF_3Br and inert gases is caused by an increased chemical inhibition effectiveness of CF_3Br as the flame temperature decreases because of the inert component of the binary mixture.

To verify the above suggestion, we recently performed a numerical investigation on the temperature sensitivity of inhibition effectiveness of CF_3Br in one-dimensional methane-oxygen-inert freely propagating flames [10]. The results demonstrated that the inhibition effectiveness of CF_3Br is enhanced at lower flame temperatures due to the enhanced catalytic inhibition cycles. Figure 1 shows the regeneration coefficient of Br as a function of adiabatic flame temperature computed for $7.5\%CH_4$-$15\%O_2$-$1\%CF_3Br$-N_2-Ar mixtures. The regeneration coefficient K_r is defined by Noto et al. [2] as

$$K_r = \frac{\int \sum_i w_{X,i} dt}{C_{\text{suppressant}}} \tag{1}$$

Here $w_{X,i}$ is the rate of the i th reaction which consumes the scavenging agent X (HBr), and $C_{\text{suppressant}}$ is the initial concentration of the suppressant which generates the agent X. Thus, a larger value of K_r means a higher cycle efficiency [2, 10]. Also plotted in Fig. 1 is the residence time in the regeneration reaction zone, that is defined as the region where the total regeneration reaction rate exceeds 10% of its maximum. As seen in Fig. 1, the catalytic inhibition cycles are enhanced at lower flame temperatures, due to thicker reaction zone and hence longer residence time. Based on this finding, we attributed the synergism between CF_3Br and inert gases to more efficient catalytic cycles at lower temperatures.

The experimentally observed synergism between CF_3Br and inert gases are, however, measured by premixed tubular flame [7] and the cup-burner diffusion flame extinction experiments [6,8,9], where the flames are not allowed to be thickened infinitely as in the ideal freely-propagating flames examined numerically. Therefore it is necessary to further investigate the catalytic inhibition cycles of CF_3Br to thoroughly understand the temperature sensitivity in actual flames. The objective of the present study is to verify the applicability of the previous finding of one-dimensional freely propagating flames to counterflow diffusion flames in that the residence time in reaction zone is restricted. We first demonstrate numerically that the similar synergistic effect between CF_3Br and N_2 on inhibition effectiveness can be reproduced for the extinction condition of methane-air diffusion flames when the binary suppressant is doped in the oxidizer mixture, using the same kinetic model as employed in the previous study. We then performed a systematic computational experiment which demonstrates the effect of flame temperature on the efficiency of catalytic inhibition cycles by CF_3Br, employing K_r as the relevant measure. In addition, we examined the effects of strain rate and suppressant concentration on the efficiency of catalytic cycles.

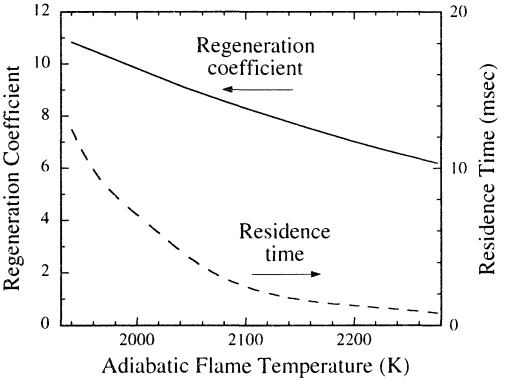

FIGURE 1. Variations of the regeneration coefficient of Br and the residence time for premixed 7.5% CH_4 - 15%O_2 - 1% CF_3Br - N_2 - Ar freely propagating flames, as a function of flame temperature.

Because the flame temperature, strain rate, and suppressant concentration are all coupled with one another in a flame, each effect is isolated systematically to investigate the individual effects. Following the work of Du et al. [11], the variation of flame temperature in these computational experiments is achieved by substituting nitrogen in the oxidizer mixture by argon, without having to change the oxygen and suppressant compositions in the oxidizer mixture. The chemical kinetic effects which cause the enhancement of the catalytic cycles at lower temperatures are discussed. We shall also demonstrate the enhanced efficiency of catalytic cycles at lower strain rates and smaller suppressant doping.

NUMERICAL CALCULATIONS

The kinetic model employed in the present study is the same as that used in Ref. 10. The base model of C-H-O-F was based on GRI-Mech 1.2 [12] and the work of Burgess et al. [13]. Several rate parameters in the kinetic model by Burgess et al. [13] were modified on the basis of more recent experimental measurements and to better predict the laminar burning velocities for CH_4-CHF_3-air mixtures [14]. The reaction kinetics relevant to CF_3Br are taken from the work of Noto et al. [15]. The combined kinetic model consists of 75 species and 591 reaction steps. We note that the inhibition chemistry in this model has been poorly verified experimentally with non-premixed flames. Truett et al. [4] tested a similar inhibition model against the extinction conditions of non-premixed hydrogen flames doped with CF_3Br, and found that the model underpredicts the inhibition effectiveness of CF_3Br. With all uncertainties remaining, however, the present model reproduced qualitatively the synergism between CF_3Br and inert gases on suppresstion effectiveness [10], that was experimentally observed for diffusion flame [6]. It is not surprising, because the synergism is due to the existence of an effective catalytic inhibition cycle, that is characteristic of CF_3Br chemistry. Recognizing that the objective of the present study is to reveal how the catalytic inhibition cycle can cause the synergism in non-premixed configuration, uncertainties in the kinetic model should not affect the conclusion seriously.

Figure 2 shows the schematic illustration of the axisymmetric steady counterflow flat diffusion flame stabilized between opposed fuel and oxidizer nozzles. The mathematical model and the governing equations follow that of Kee et al. [16] and Dixon-Lewis [17]. Thermochemical and transport properties were calculated with CHEMKIN II [18] and the transport subroutine package of Ref. 19, respectively. For consistency, the transport database was taken from the GRI-Mech [12] for C-H-O species and from Refs. 15 and 13 for Br- and F-containing species, respectively. Computations were performed for atmospheric pressure flames with fuel and oxidizer temperature of 298 K, over a domain of 1.5 cm and with central differencing for the convective terms, employing adaptive gridding with the total number of grid points between 150-230. At both ends of the computational domain the radial component of the flow velocity is set equal to zero, and the axial component of the flow velocity u is set at either 40 or 80 cm/s.

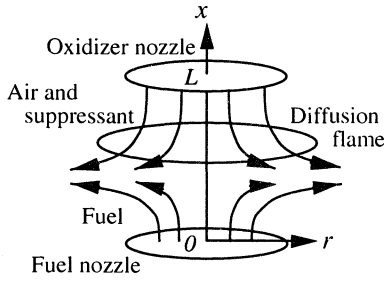

FIGURE 2. Schematic illustration of the counterflow diffusion flame.

Computational Experiments

To demonstrate the synergism of binary CF_3Br -N_2 suppressant, computations were performed for CH_4-air counterflow diffusion flames doped with various compositions of the binary suppressant at the oxidizer side. To obtain the extinction curves as a function of the concentration of the binary suppressant at a constant fuel and oxidizer velocity, the flame-controlling continuation method by Nishioka et al. [20] was employed with a boundary condition modified to obtain the concentration of suppressant instead of the strain rate in Ref. 20.

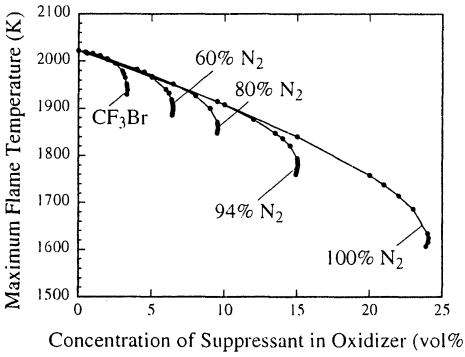

FIGURE 3. Variation of the maximum flame temperatures of methane-air counterflow diffusion flames doped with CF_3Br-N_2 binary suppressants, as a function of the concentration of binary suppressant in the oxidizer mixture.

Examples of the extinction curves computed for the case of u = 40 cm/s are presented in Figure 3. The extinction concentration of suppressant can be defined as the maximum concentration on the extinction curve, that connects the upper and middle branches of the multiple solutions.

To investigate individually the effects of flame temperature, strain rate, and the magnitude of suppressant doping on the efficiency of catalytic cycles with Br species, computations are performed for methane versus 1%CF_3Br-18%O_2-inert (N_2+Ar) and 0.5%CF_3Br-18%O_2-inert (N_2+Ar) mixtures as oxidizer. For the case of 1%CF_3Br-18%O_2-inert (N_2+Ar) oxidizer, two different u values of 40 cm/s and 80 cm/s are set for the computations. At a fixed level of CF_3Br addition, the maximum flame temperature is varied by manipulating the relative concentration of nitrogen and argon in the oxidizer mixture.

RESULTS AND DISCUSSION

Synergistic Effect of Binary CF_3Br and N_2 Suppressant

We first demonstrate that the synergistic effect between CF_3Br and N_2 on inhibition effectiveness is well reproduced by the model for the extinction condition of methane-air diffusion flames. Fig. 3 presents the variation of maximum flame temperatures as a function of suppressant concentration added to the oxidizer, computed at u = 40 cm/s. The suppressants presented in Fig. 3 are binary CF_3Br-N_2 mixtures with three different compositions as well as pure CF_3Br and N_2. The critical concentrations at extinction for CF_3Br and N_2 are found to be 3.34 % and 24.1 %, respectively. Using these values, the critical extinction concentrations of the binary suppressants can be interpreted by plotting an interaction index, I_s, as a function of the concentration of N_2 in the binary suppressant, as shown in Figure 4a. Here I_s is defined as $I_s = C_{b,obs}/C_b$ where $C_{b,obs}$ is the observed critical extinction concentration of a binary suppressant, and C_b represents the expected critical extinction concentration [21],

$$C_b = \left[\frac{X_1}{C_{s,1}} + \frac{X_2}{C_{s,2}} \right]^{-1} \qquad (2)$$

where X_i is the mole fraction of the i th component in the binary suppressant mixture ($X_1 + X_2 = 1$), and $C_{s,i}$ is the critical concentration at extinction of the i th component when it is used alone. If there is no interaction between the two components or if the interaction does not cause any synergism, $C_{b,obs} = C_b$ and $I_s = 1$. If there is a positive interaction or synergism, $C_{b,obs}$ must be smaller than C_b, and thus $I_s < 1$. Also shown in Fig. 4a is the numerically obtained maximum flame temperature at the extinction turning point. It is seen that I_s is less than unity,

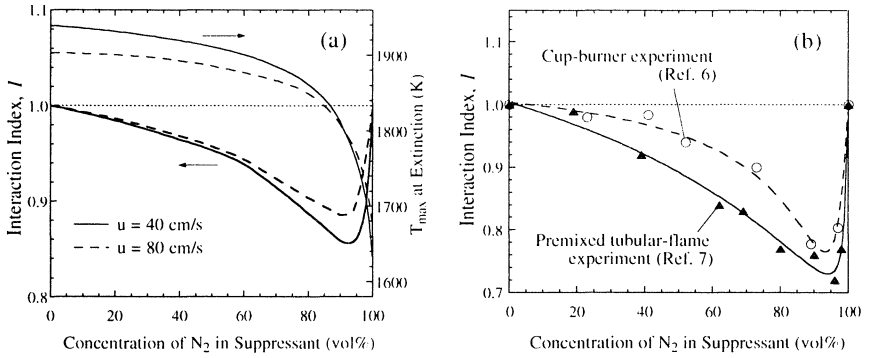

FIGURE 4. Variations of the interaction index of binary CF_3Br-N_2 suppressant obtained through (a) the computed extinction condition of the methane-air counterflow diffusion flame, and (b) the cup-burner flame [6] and the premixed tubular-flame [7] extinction experiments, as a function of the concentration of N_2 in the binary suppressant.

indicating a positive synergism between CF_3Br and N_2 in the counterflow diffusion flame. The most significant interaction is seen for the lower velocity case with the smallest I_s equal to 0.86, at a small concentration of CF_3Br in the suppressant mixture where the flame temperature is lower than at larger CF_3Br concentrations. These results agree well with the previous experimental observations shown in Figure 4b, and with the computational study [10] in which the synergistic effect was attributed to the temperature sensitivity of CF_3Br inhibition effectiveness due to more efficient catalytic inhibition cycles at lower flame temperatures.

To interpret the results of Fig. 4a, the regeneration coefficient K_r for Br atom and the residence time in reaction zone at extinction are calculated. K_r can be obtained with Eq.(1), and the residence time is calculated by integrating the inverse of the flow velocity at each grid. The residence time becomes infinity if the integration is performed over the entire domain including the stagnation surface. Thus in the present study, the integration to obtain K_r and the residence time is performed within the range where the sum of the regeneration reaction rates exceeds 10^{-6} mol/cm^3/s, which corresponds to approximately 1% to 0.1% of the maximum total regeneration rate. The results are plotted as a function of the maximum flame temperature in Figure 5. It is seen that K_r increases with a decrease in temperature, which is consistent with the previous results for the freely propagating flames. However, the residence time in Fig. 5 is quite insensitive to the flame temperature, while that for the freely propagating flame is remarkably sensitive as shown in Fig. 1. This is because the residence time in the counterflow flame is controlled primarily by the magnitude of the forced-convection, while there exists no forced-convection in the case of freely-propagating flame. Therefore the temperature sensitivity of K_r observed for the counterflow diffusion flame cannot be explained by the residence time effect.

When we compare the results between two different velocity cases in Figs. 4a and 5, it is found that the synergistic effect is less significant at higher velocity while K_r is larger. Because the maximum temperature of the uninhibited flame is reduced with an increase in strain rate, higher velocity causes smaller difference in flame temperature between extinction by CF_3Br and by N_2. Consequently, the effect of N_2 addition becomes less significant, resulting in the smaller synergism at the higher velocity seen in Fig. 4a. Simultaneously the higher velocity causes a lower concentration of CF_3Br at extinction. The numerically obtained critical concentration at

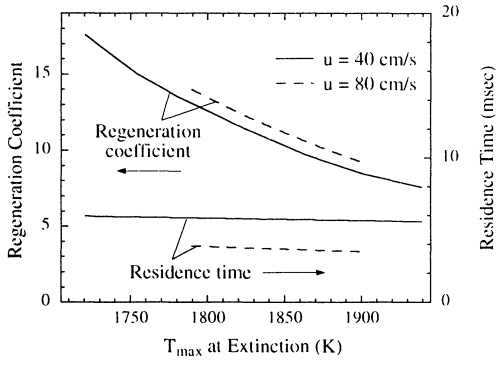

FIGURE 5. Variations of the regeneration coefficient of Br and the residence time in the reaction zone as a function of the maximum flame temperature at the extinction turning point as shown in Fig. 3.

extinction for pure CF_3Br is 1.97 % at u = 80 cm/s, that is about 60% of the u = 40 cm/s case. It is well known that one of the significant characteristics of catalysis is higher performance at small doping. Because the concentration of CF_3Br in the oxidizer at extinction also varies with the composition of the binary suppressant, the results shown in Fig. 5 are the consequence of the flame temperature, the strain rate, and the suppressant concentration effects all coupled together.

Effect of Flame Temperature on the Efficiency of Catalytic Cycles by CF_3Br

We next isolate the individual effects of the flame temperature, strain rate, and suppressant concentration to investigate the pure temperature sensitivity of the regeneration coefficient. At a fixed level of CF_3Br addition, the maximum flame temperature is varied by manipulating the relative concentration of nitrogen and argon in the oxidizer mixture. The maximum flame temperatures as a function of substituted argon are presented in Figure 6. We note that in Fig. 6, the left ends of the plots for the cases of 1% CF_3Br addition are near extinction conditions, while the extinction does not occur within the range of Fig. 6 for the case of 0.5% CF_3Br addition. Within the temperature range investigated, the computed local strain rates were found to have negligible variation at a constant reactant-flow velocity.

Figure 7 presents the regeneration coefficient and residence time in the reaction zone as a function of the maximum flame temperature, computed at a constant u for constant concentra-

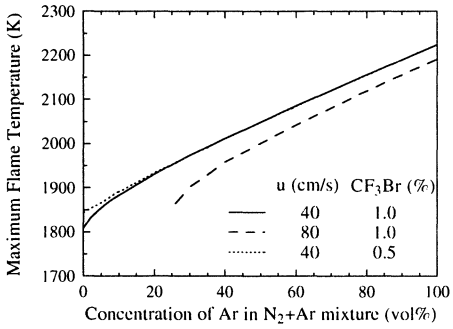

FIGURE 6. Variation of the maximum flame temperature as a function of the concentration of Ar in the N_2-Ar inert component in the oxidizer. The concentration of O_2 in the oxidizer is fixed at 18%.

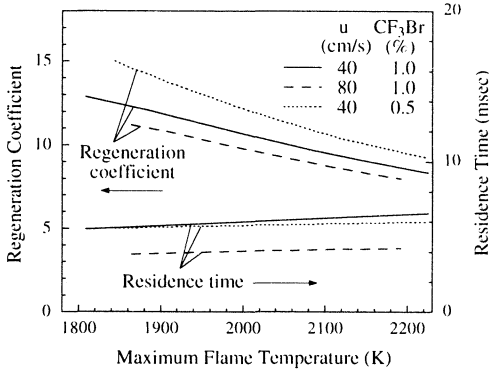

FIGURE 7. Variations of the regeneration coefficient of Br and the residence time in the reaction zone as a function of the maximum flame temperature computed for a methane versus 18%O_2-CF_3Br-N_2-Ar counterflow diffusion flame. The conditions correspond to that of Fig. 6.

tions of O_2 and CF_3Br in the oxidizer. In all cases, K_r increases with a decrease in the flame temperature, while the residence time remains unchanged. These findings agree qualitatively with the results in Fig. 5, thus demonstrating the contribution of the temperature sensitivity of K_r to the observed synergism between CF_3Br and N_2. Quantitatively, however, the temperature sensitivity of K_r in Fig. 7 is less significant than the results in Fig. 5, suggesting that there also exists a concentration effect in the synergism shown in Fig. 4. The effect of suppressant concentration will be discussed later.

Eq. (1) shows that K_r is determined by both the residence time in the reaction zone and the rates of regeneration reactions. In the freely propagating flames previously investigated, the temperature sensitivity of K_r is caused by significant differences in the residence time, while the Br regeneration reaction rates decrease with a decrease in flame temperature. In the counterflow diffusion flames, however, the temperature sensitivity of K_r is caused by an increased Br regeneration rates at lower flame temperatures, while the residence time remains unchanged at a constant u.

Figures 8a and 8b respectively present the temperature profiles and the total rate profiles of Br-atom regeneration, computed with three different flame temperatures. It is seen in Fig. 8b that there are two peaks in the regeneration rate profiles, with the primary peak at the location of the maximum temperature and the secondary peak at the oxidizer side of the flame. The primary peak shows a significant sensitivity to the maximum flame temperature, while the secondary peak is quite insensitive to the maximum temperature because of little variation in temperature at the oxidizer side of the flame as shown in Fig. 8a. Shown in Figure 8c are the mole fraction profiles of Br, HBr, and Br_2. It is seen that the secondary peak in Fig. 8b is located at the region where Br atoms are produced, while the primary peak is located at the region where Br atoms are consumed. The catalytic inhibition is inefficient between the two peaks, that is reflected in the plateau-like profile of Br shown in Figure 8c and the maximum concentrations of H, O, and OH located in this region. A similar plateau-shaped profile of Br was reported previously by Trees et al. [3], although it was explained as a consequence of fast reactions involving Br and HBr, that did not cause a significant change in the overall Br concentration. The present results show no remarkable reactions involving Br and HBr in the plateau region, which is inconsistent with their explanation.

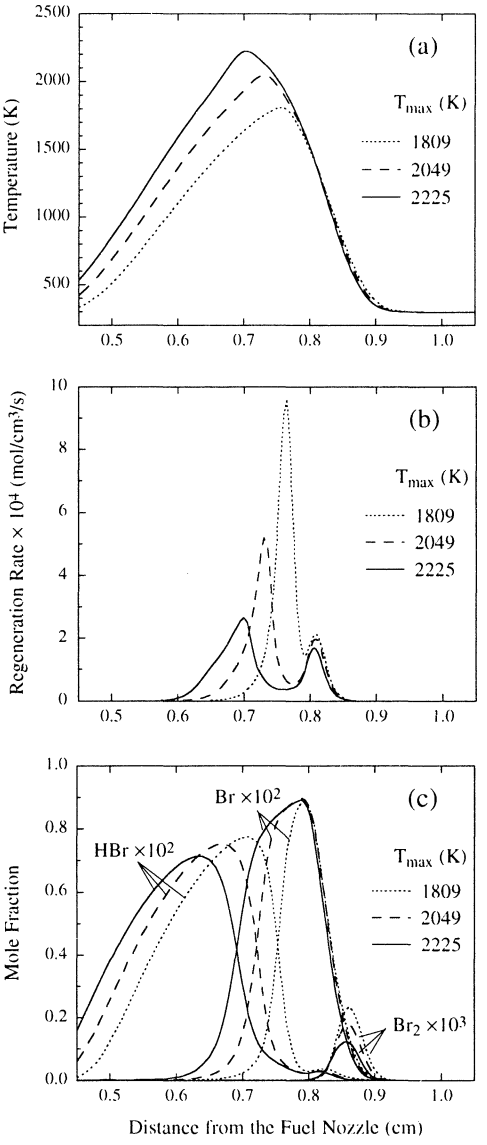

FIGURE 8. (a) The temperature profiles, (b) the total rate profiles of Br regeneration reactions, and (c) the mole fraction profiles of important Br species, computed for the case of u = 40 cm/s and 1% CF_3Br in Fig. 6.

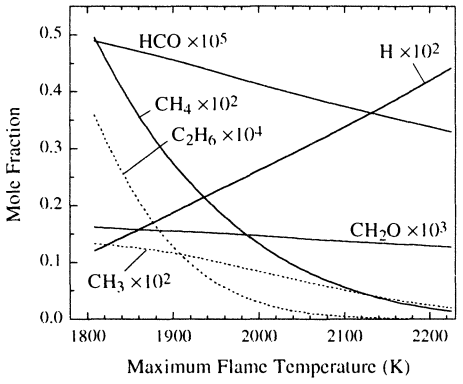

FIGURE 9. Variations of the peak mole fractions of H, HCO, CH_2O and the mole fractions at the location of the maximum flame temperature for CH_4, CH_3 and C_2H_6, as a function of the maximum flame temperature. The conditions correspond to that of u = 40 cm/s and 1% CF_3Br in Fig. 6.

The secondary peak in Fig. 8b is found to be a consequence of the following reactions,

$CF_3Br + H$	$\rightarrow$	$CF_3 + HBr$	(R1)
$HBr + OH$	$\rightarrow$	$Br + H_2O$	(R2)
$Br + Br + M$	$\rightarrow$	$Br_2 + M$	(R3)
$H + Br_2$	$\rightarrow$	$HBr + Br$	(R4)

The primary peak is a consequence of the following reactions:

$HBr + H$	$\rightarrow$	$Br + H_2$	(R5)
$Br + HCO$	$\rightarrow$	$HBr + CO$	(R6)
$Br + CH_2O$	$\rightarrow$	$HBr + HCO$	(R7)
$Br + CH_4$	$\rightarrow$	$HBr + CH_3$	(R8)
$Br + C_2H_6$	$\rightarrow$	$HBr + C_2H_5$	(R9)

At the location of the primary peak, reaction (R5) leads to HBr consumption, while reactions (R6)-(R9) are the HBr regeneration reactions. All rate profiles of the reactions (R5)-(R9) are found to be approximately equally sensitive to the maximum flame temperature.

Figure 9 presents the maximum mole fractions of H, HCO and CH_2O as well as the mole fractions at the location of the maximum flame temperature for CH_4, CH_3 and C_2H_6, as a function of the maximum flame temperature. It is seen that the mole fractions of all species except for the H atom increase with a decrease in temperature. Especially the increase of CH_4 is quite significant. These results are in contrast to that of the freely propagating flames in which the mole fractions of the intermediate species such as HCO decrease markedly with a decrease in flame temperature, approximately proportional to that of the H atom. Through these analyses, the temperature sensitivity of K_r in the counterflow diffusion flame can be attributed to the enhancement of reactions (R6)-(R9) due to the slower oxidation of the fuel at lower flame temperature and resulting in higher concentrations of fuel and fuel-originated intermediates at the regeneration reaction zone, that are important for regeneration of HBr from Br. Thus the fundamental aspect is the same between the counterflow diffusion flame and the premixed freely propagating flame, that is, the catalytic inhibition cycles are more effective with slower combustion reactions.

To further validate the above explanation, some brute-force sensitivity analyses are performed for the temperature sensitivity of K_r. When reactions (R6) and (R7) are removed from the kinetic model, not only K_r values but also the temperature sensitivity of K_r are reduced significantly. Furthermore, removing reactions (R6), (R7), and (R8) causes negligible temperature sensitivity of K_r, which supports the above suggestions.

We note that the sensitivity of individual reactions to K_r does not necessarily represent the flame inhibition effectiveness of each reaction. Although K_r is a useful measure in examining the global behavior of catalytic cycles, it seems not to be an appropriate measure of the net inhibition effectiveness, since some of the scavenger-regenerating pathways may promote combustion. For example, removing the reaction (R8) from the kinetic model results in enhanced inhibition effectiveness of CF_3Br, since the reaction (R8) promotes the combustion through competition with the reaction (R6).

Effects of Strain Rate and Suppressant Concentration

Comparing the results of u = 40 cm/s and 80 cm/s in Fig. 7, we find that the higher strain rate reduces the effectiveness of the regeneration cycle because of the shorter residence time. However, the reduction of K_r is insignificant as compared to the reduction of the residence time. This is because the total regeneration rate is greater at higher strain rate, due to the higher concentrations of CH_4, HCO, etc. at the regeneration zone even with compensating the temperature reduction. As a result, the effect of strain rate on K_r is smaller than the other effects.

The effect of suppressant concentration on K_r can be evaluated by comparison between the results of 1% CF_3Br and 0.5% CF_3Br at u = 40 cm/s in Fig. 7. It is seen that the smaller doping of CF_3Br causes markedly larger K_r, because the $C_{suppressant}$ term in Eq. (1) decreases. Although the total regeneration rate is lower at smaller doping of CF_3Br, the effectiveness of the regeneration cycles per one molecule of CF_3Br is higher with less CF_3Br doping. Higher performance at small doping is known as a characteristic of catalysis. The reduced effectiveness at higher suppressant concentration is also consistent with a recent finding by Noto et al. [2], which demonstrated saturation of chemical effect. We note that the saturation of chemical effect is observed for both catalytic and non-catalytic halogenated suppressants in Ref. 2, while the effect of suppressant concentration on K_r demonstrated here is specific to catalytic suppressants.

Recognizing these effects, we note that the greater K_r at u =80 cm/s in Fig. 5 can be explained as the insignificant strain effect overcome by the suppressant concentration effect.

SUMMARY

Effects of flame temperature, strain rate, and suppressant concentration in the oxidizer on the efficiency of catalytic inhibition cycles by CF_3Br in methane-air counterflow diffusion flames are numerically investigated with detailed chemistry and transport, employing the regeneration coefficient as the relevant measure. The synergistic effect between CF_3Br and N_2 on the inhibition effectiveness is found to be well reproduced numerically for the extinction condition of methane-air diffusion flames, indicating the temperature sensitivity of CF_3Br effectiveness in the counterflow diffusion flames. Systematic computational experiments are then conducted to

isolate the individual effect of flame temperature, strain rate, and suppressant concentration on the efficiency of catalytic inhibition cycles by CF_3Br. Computational results are compared with the previous findings of one-dimensional freely propagating flames, in which the efficiency of catalytic inhibition cycles with Br species is markedly enhanced at lower flame temperatures because of significantly longer residence time in the reaction zone. The present results at constant strain rates demonstrate that the efficiency of inhibition cycles in the counterflow flame is enhanced at lower flame temperatures, while the residence time remains unchanged with the flame temperature variation. The enhanced efficiency in the counterflow flame is attributed to slower oxidation resulting in higher concentrations of fuel-originated species in the catalytic reaction zone, which are important for regeneration of HBr from Br. At a constant flame temperature, the efficiency of inhibition cycles is found to be greater at smaller strain rates and suppressant doping.

Acknowledgments

The authors thank Professor Makihito Nishioka of the University of Tsukuba for the use of his computer code, and Dr. Takashi Noto of NKK Corporation for helpful discussion on the computation of the regeneration coefficient. This work was supported by the Science and Technology Agency of Japan.

REFERENCES

1. Westbrook, C. K., *Combust. Sci. and Tech.* 34: 201-225 (1983).
2. Noto, T., Babushok, V., Hamins, A., and Tsang, W., *Combust. Flame* 112: 147-160 (1998).
3. Trees, D., Grudno, A., and Seshadri, K., *Combust. Sci. and Tech.*, 124:311-330 (1997).
4. Truett, L., Thermann, H., Trees, D., Seshadri, K., Yuan, J., Wells, L., and Marshall, P., *Twenty-Seventh Symposium (International) on Combustion*, The Combustion Institute, Pittsburgh, 1998, pp. 2741-2748.
5. Casias, C. R. and McKinnon, J. T., *Twenty-Seventh Symposium (International) on Combustion*, The Combustion Institute, Pittsburgh, 1998, pp. 2731-2739.
6. Saito, N., Saso, Y., Ogawa, Y., Otsu, Y., and Kikui, H., *Fire Safety Science - Proceedings of the Fifth International Symposium*, International Association for Fire Safety Science, 1997, pp.901-910.
7. Ogawa, Y., Saito, N., and Saso, Y., *Proceedings of Halon Options Technical Working Conference*, Albuquerque, NM, May 6-8, 1997, pp. 106-115.
8. Lott, J. L., Christian, S. D., Sliepcevich, C. M. and Tucker, E. E., *Fire Technol.* 32: 260-271 (1996).
9. Sheinson, R. S. and Maranghides, A., *Proceedings of Halon Options Technical Working Conference*, Albuquerque, NM, May 6-8, 1997, pp. 19-30.
10. Saso, Y., Ogawa, Y., Saito, N., and Wang, H., *Combust. Flame* 118: 489-499 (1999).
11. Du, D.X., Axelbaum, R.L., and Law, C.K., *Twenty-Third Symposium (International) on Combustion*, The Combustion Institute, Pittsburgh, 1990, pp.1501-1507.
12. Frenklach, M., Wang, H., Bowman, C. T., Hanson, R. K., Smith, G. P., Golden, D. M., Gardiner, W. C., and Lissianski, V., An Optimized Kinetic Model for Natural Gas Combustion, *Twenty-Fifth International Symposium on Combustion*, Irvine, California, 1994, Work-In-Progress Poster Session 3, Number 26.
13. Burgess, D.R.F., Jr., Zachariah, W., Tsang, W. and Westmoreland, P.R., *Prog. Energy*

Combust. Sci. 21: 453-529 (1996).
14. Saso, Y., Zhu, D. L., Wang, H., Law, C. K., and Saito, N., *Combust. Flame* 114: 457-468 (1998).
15. Noto, T., Babushok, V., Burgess, D.R.F.,Jr., Hamins, A., Tsang, W. and Miziolek, A., *Twenty-Sixth Symposium (International) on Combustion*, The Combustion Institute, Pittsburgh, 1996, pp.1377-1383.
16. Kee, R. J., Miller, J. A., Evans, G. H. and Dixon-Lewis, G., *Twenty-Second Symposium (International) on Combustion*, The Combustion Institute, Pittsburgh, 1988, pp.1479-1494.
17. Dixon-Lewis, G., *Twenty-Third Symposium (International) on Combustion*, The Combustion Institute, Pittsburgh, 1990, pp.305-324.
18. Kee, R. J., Rupley, F. M. and Miller, J. A., Sandia Report SAND 89-8009B, Sandia National Laboratories, Albuquerque, NM, 1989.
19. Kee, R. J., Warnatz, J. and Miller, J. A., Sandia Report SAND 83-8209, Sandia National Laboratories, Albuquerque, NM, 1983.
20. Nishioka, M., Law, C. K. and Takeno, T., *Combust. Flame* 104: 328-342 (1996).
21. Saito, N., Ogawa, Y., Saso, Y., Liao, C., and Sakei, R., *Fire Safety J.* 27: 185-200 (1996).